SCAMP5 plays a critical role in axonal trafficking and synaptic localization of NHE6 to adjust quantal size at glutamatergic synapses

Unghwi Lee[a], Chunghon Choi[a], Seung Hyun Ryu[a], Daehun Park[a,1], Sang-Eun Lee[a,b], Kitae Kim[a], Yujin Kim[a,b], and Sunghoe Chang[a,b,2]

[a]Department of Physiology and Biomedical Sciences, Seoul National University College of Medicine, Seoul 03080, South Korea; and [b]Neuroscience Research Institute, Seoul National University College of Medicine, Seoul 03080, South Korea

Edited by Robert H. Edwards, University of California, San Francisco, CA, and approved November 30, 2020 (received for review June 5, 2020)

Glutamate uptake into synaptic vesicles (SVs) depends on cation/H^+ exchange activity, which converts the chemical gradient (ΔpH) into membrane potential (Δψ) across the SV membrane at the presynaptic terminals. Thus, the proper recruitment of cation/H^+ exchanger to SVs is important in determining glutamate quantal size, yet little is known about its localization mechanism. Here, we found that secretory carrier membrane protein 5 (SCAMP5) interacted with the cation/H^+ exchanger NHE6, and this interaction regulated NHE6 recruitment to glutamatergic presynaptic terminals. Protein–protein interaction analysis with truncated constructs revealed that the 2/3 loop domain of SCAMP5 is directly associated with the C-terminal region of NHE6. The use of optical imaging and electrophysiological recording showed that small hairpin RNA–mediated knockdown (KD) of SCAMP5 or perturbation of SCAMP5/NHE6 interaction markedly inhibited axonal trafficking and the presynaptic localization of NHE6, leading to hyperacidification of SVs and a reduction in the quantal size of glutamate release. Knockout of NHE6 occluded the effect of SCAMP5 KD without causing additional defects. Together, our results reveal that as a key regulator of axonal trafficking and synaptic localization of NHE6, SCAMP5 could adjust presynaptic strength by regulating quantal size at glutamatergic synapses. Since both proteins are autism candidate genes, the reduced quantal size by interrupting their interaction may underscore synaptic dysfunction observed in autism.

NHE6 | SCAMP5 | presynaptic terminal | quantal size | autism

The uptake of classical transmitters into synaptic vesicles (SVs) depends on a proton electrochemical gradient ($\Delta\mu H^+$), consisting of the chemical gradient (ΔpH) and membrane potential (Δψ) across the SV membrane (1). $\Delta\mu H^+$ is generated by vacuolar-type H^+-ATPases and ion channels/transporters on SVs (2). There are five classes of vesicular neurotransmitter transporters on SVs, namely, vesicular glutamate transporters (VGLUT 1 to 3), vesicular GABA/glycine transporter (VGAT, VIAAT), vesicular monoamine transporters (VMAT 1, 2), vesicular acetylcholine transporter (VAChT), and vesicular nucleotide transporter (VNUT); these all use ΔpH and Δψ, but to different extents, to fill SVs with neurotransmitters (3). For example, transporters for the anionic neurotransmitter, glutamate, mainly utilize Δψ, whereas the transporters for the cationic neurotransmitter, acetylcholine, and zwitterionic neurotransmitters, GABA and glycine, depend on ΔpH and both ΔpH and Δψ, respectively (4). Therefore, homeostatic regulation of $\Delta\mu H^+$ is important for controlling the quantal size of neurotransmitter release.

Cation/H^+ exchange activity across the membrane is mostly attributed to monovalent $Na^+(K^+)/H^+$ exchangers (NHEs) that present at the plasma membrane or intracellular organelles (5). In humans, the NHE superfamily comprises nine isoforms consisting of NHE1 to NHE5 on the plasma membrane, NHE6 and NHE9 on intracellular vesicles, and NHE7 and NHE8 on the Golgi apparatus (6). Plasma membrane isoforms recognize Na^+ but not K^+ and have important roles in the regulation of cytoplasmic pH, while the intracellular isoforms recognize K^+ as well as Na^+ (7), but their physiological roles remain poorly understood. Loss-of-function mutations of NHE6 and NHE9, the two endosomal subtypes (eNHEs), are implicated in multiple neurodevelopmental and neuropsychiatric disorders, including autism, Christianson syndrome, X-linked intellectual disability, and Angelman syndrome (8–13). NHE6 and NHE9 are highly expressed in the brain, including the hippocampus and cortex (14). Previous studies have found that SVs show an NHE activity that plays an important role in glutamate uptake into SVs by dissipating ΔpH and increasing Δψ (15, 16), and thus, eNHEs were considered to reside in SVs to perform this function (14). However, it was found that there was no defect in vesicular filling with glutamate or GABA in NHE9 knockout (KO) neurons, and NHE9 regulated the luminal pH of axonal endosomes rather than recycling SVs (17). In contrast, NHE6 was identified on SVs by using quantitative proteomics (18), and its presynaptic localization was shown by immunofluorescent analysis (19). In addition, more severe synaptic dysfunction was observed in NHE6 KO mice (19) than in NHE9 KO mice (17). These results suggest that NHE6 and NHE9 are not functionally redundant, and NHE6 is responsible for NHE activity in SVs that regulates glutamate uptake at presynaptic terminals. Evidently, the proper localization of NHE6 to SVs is of utmost importance in determining the glutamate

Significance

As a vesicular $Na^+(K^+)/H^+$ exchanger, NHE6 promotes glutamate filling into synaptic vesicles (SVs). Thus, proper localization of NHE6 is critical for determining synaptic strength at glutamatergic synapses, but the underlying mechanism remains unknown. We found that an SV-enriched protein, SCAMP5, is a key determinant for axonal trafficking and synaptic localization of NHE6. By perturbing their interaction, NHE6 fails to be localized at synaptic sites, resulting in hyperacidification of the SV lumen and a significant reduction in the quantal size of glutamate released. Since both are autism candidate genes, our results suggest that impaired interaction between two proteins could relate to the synaptic dysfunction observed in autism.

Author contributions: U.L. and S.C. designed research; U.L., C.C., S.H.R., D.P., S.-E.L., K.K., and Y.K. performed research; U.L. and S.C. analyzed data; and U.L., S.-E.L., and S.C. wrote the paper.

The authors declare no competing interest.

This article is a PNAS Direct Submission.

[1]Present address: Department of Cell Biology, Yale University School of Medicine, New Haven, CT 06510.

[2]To whom correspondence may be addressed. Email: sunghoe@snu.ac.kr.

This article contains supporting information online at https://www.pnas.org/lookup/suppl/doi:10.1073/pnas.2011371118/-/DCSupplemental.

Published December 28, 2020.

quantal size, but the mechanism underlying NHE6 recruitment to SVs is mostly unknown.

Secretory carrier membrane proteins (SCAMPs) are known to regulate vesicular trafficking and vesicle recycling processes. Of the five known SCAMPs, SCAMP1 and SCAMP5 are highly expressed in the brain and enriched in SVs (20). The study of SCAMP1 KO mice showed that it was not necessary for brain function and synaptic physiology (21), suggesting a critical role of SCAMP5 in synaptic function. Indeed, a recent genetic analysis showed that SCAMP5 was silenced on a derivative chromosome and was reduced in expression to ~40% of normal in a patient with idiopathic, sporadic autism (22), and several SCAMP5 mutations reported in humans have been implicated in neurodevelopmental and neurodegenerative disorders such as intellectual disability, seizure, and Parkinson's disease (23, 24). We also have provided evidence that SCAMP5 plays a critical role in SV endocytosis during strong neuronal activity (25) and the protein clearance at the presynaptic SV release site (26). These results suggest that SCAMP5 plays an important role in regulating the function and trafficking of synaptic proteins at presynaptic terminals.

In this study, we showed that SCAMP5 directly interacted with NHE6. Optical imaging and electrophysiological recordings proved that when perturbing their interaction, axonal trafficking and synaptic localization of NHE6 were severely impaired, which subsequently lowered the resting luminal pH of SVs and reduced the amounts of glutamate release. Knockout of NHE6 occluded the effect of SCAMP5 knockdown (KD) without causing additional defects. Since NHE6 and SCAMP5 are candidate genes for autism (9, 22), the reduced quantal size following impairment of their interaction may relate to the synaptic dysfunction observed in autism.

Results

TM2-2/3-TM3 Domain of SCAMP5 Directly Interacts with the C-Terminal Region of NHE6. Our previous results showed that SCAMP5 is highly enriched in SVs and plays a role in vesicular trafficking at presynaptic terminals (25, 26). Since several studies reported that other SCAMP isoforms, SCAMP1 and SCAMP2 interacted with the plasma membrane and Golgi resident NHE isoforms, NHE5 and NHE7, respectively (27, 28), we reasoned that SCAMP5 could interact with NHE6 at the presynaptic terminals. To identify the interaction between SCAMP5 and NHE6, we performed coimmunoprecipitation assays and found that endogenous NHE6 and SCAMP5 interacted with each other (*SI Appendix*, Fig. S1 *A* and *B*). We next sought to define the NHE6-interacting domain of SCAMP5 (Fig. 1*A*). None of the cytoplasmic domains of SCAMP5 (Nt cyto, 2/3 cyto, and Ct cyto) bound to NHE6, whereas full-length SCAMP5 (SC5 FL) did (Fig. 1*B* and *SI Appendix*, Fig. S2*A*). Neither the N-terminal cytoplasmic domain containing the first transmembrane region (Nt-TM1) nor the C-terminal cytoplasmic domain containing the fourth transmembrane region (TM4-Ct) of SCAMP5 bound to NHE6, whereas the cytoplasmic 2/3 loop flanked by a transmembrane region at both its N and C termini (TM2-2/3-TM3) did (Fig. 1*C* and *SI Appendix*, Fig. S2*A*). The 2/3 loop domain with only the N- or C-terminal transmembrane region (TM2-2/3 or 2/3-TM3) also failed to bind to NHE6 (Fig. 1*D* and *SI Appendix*, Fig. S2*A*), indicating that both transmembrane regions flanking the cytoplasmic 2/3 loop are critical for the interaction between SCAMP5 and NHE6. These findings were further corroborated by the results in which the full-length SCAMP5 containing 14 randomly scrambled amino acids in the 2/3 loop domain (SC5 FL 2/3 scr) failed to bind to NHE6 (Fig. 1*E* and *SI Appendix*, Fig. S2*A*). Since this mutant retains the protein topology of the tetra-membrane spanning structure of wild-type SCAMP5 (26), this finding indicates that the specific motif formed by TM2-2/3-TM3 is required for the interaction with NHE6.

Next, we tried to identify the SCAMP5-interacting region of NHE6 (Fig. 1*A*). NHE6 binds several proteins via its C-terminal cytoplasmic tail (29, 30). This was also the case for its interaction with SCAMP5 (Fig. 1*F* and *SI Appendix*, Fig. S2*B*). We also tested several mutations in the C-terminal region of NHE6 that had been isolated from patients with Christianson syndrome, X-linked intellectual disability, and schizophrenia (10, 11, 31). We found that nonsense mutants of NHE6 (E547X and W570X) with C-terminal tail truncations did not interact with SCAMP5, whereas the missense mutant R568Q did (Fig. 1*G* and *SI Appendix*, Fig. S2*B*). We confirmed the interaction between NHE6 and SCAMP5 by using the purified GST-tagged C-terminal cytoplasmic region of NHE6 (GST-NHE6 Ct) and 6XHis-MBP-tagged full-length wild-type SCAMP5 (6XHis-MBP-SCAMP5; Fig. 1 *H* and *I*). Collectively, these results prove that the C-terminal region of NHE6 directly binds to the TM2-2/3-TM3 domain of SCAMP5.

Knockdown of SCAMP5 or Perturbing SCAMP5–NHE6 Interaction Interferes with the Recruitment of NHE6 to SVs. Although NHE6 is known to participate in many cellular activities by modulating the luminal pH of vesicular compartments, including SVs (19, 32), there are no reports on how the localization of NHE6 to SVs is regulated. We hypothesized that SCAMP5, which is highly enriched in SVs and involved in the vesicular trafficking at synapses, could regulate the recruitment of NHE6 to SVs by their direct interaction. To check the subcellular localization of both proteins, we cotransfected cultured rat hippocampal neurons with NHE6 and SCAMP5 together with synaptophysin (SYP), an SV marker, and found that their expression patterns overlapped with that of synaptophysin (Fig. 2*A*). Furthermore, the immunoreactivity of endogenous SCAMP5 mostly overlapped with that of synaptophysin, which is consistent with our previous results (26) (*SI Appendix*, Fig. S1 *C* and *D*). The expression of endogenous NHE6 also substantially overlapped with that of vesicle-associated membrane protein 2 (VAMP2) (*SI Appendix*, Fig. S1 *E* and *F*). We next used a small hairpin RNA (shRNA) targeting SCAMP5 to suppress its expression. The efficiency of KD was demonstrated previously (25, 26) and in this study (Fig. 2 *G* and *H*). Then, cultured hippocampal neurons were cotransfected with NHE6, synaptophysin, and shRNA SCAMP5 or scrambled RNA (scrRNA). Unlike control neurons where NHE6 showed a considerable colocalization with synaptophysin (Fig. 2 *B*, *C*, and *F*), most of NHE6 failed to colocalize with synaptophysin but instead was dispersed along the axon in SCAMP5 KD neurons (Fig. 2 *D*–*F*). We confirmed that this was not due to the alteration in NHE6 expression level with SCAMP5 KD (Fig. 2 *G* and *H*). This mislocalization of NHE6 was fully rescued by an shRNA-resistant form of wild-type SCAMP5 (SC5 WT sh-resi; Fig. 2 *I*, *J*, and *M*), while an shRNA-resistant form of SCAMP5 containing the scrambled 2/3 loop sequence (SC5 2/3 scr sh-resi), which did not bind to NHE6, failed to restore the correct localization of NHE6 (Fig. 2 *K*–*M*). Accordingly, NHE6 mutants lacking the C-terminal region, which did not bind to SCAMP5, failed to colocalize with synaptophysin (*SI Appendix*, Fig. S3 *A*–*D*). Overexpression of the NHE6 C-terminal fragment in control neurons showed a dominant-negative effect on NHE6 localization (*SI Appendix*, Fig. S4 *A*–*G*). We further found that the colocalization between endogenous NHE6 and synaptophysin was significantly reduced in SCAMP5 KD neurons (*SI Appendix*, Fig. S5 *A*–*E*), while the presynaptic localization of other SV proteins such as vesicular glutamate transporter 1 (vGlut1), VAMP2, and synaptotagmin 1 (Syt1) was not affected by SCAMP5 KD (*SI Appendix*, Fig. S5 *F*–*L*), suggesting that SCAMP5 KD induces defects, especially in NHE6 localization but not in other protein localization at the presynaptic terminals.

Axonal Trafficking of NHE6 Is Significantly Impaired in SCAMP5 KD Neurons. We next investigated the detailed molecular mechanisms underlying the aberrant localization of NHE6 along the

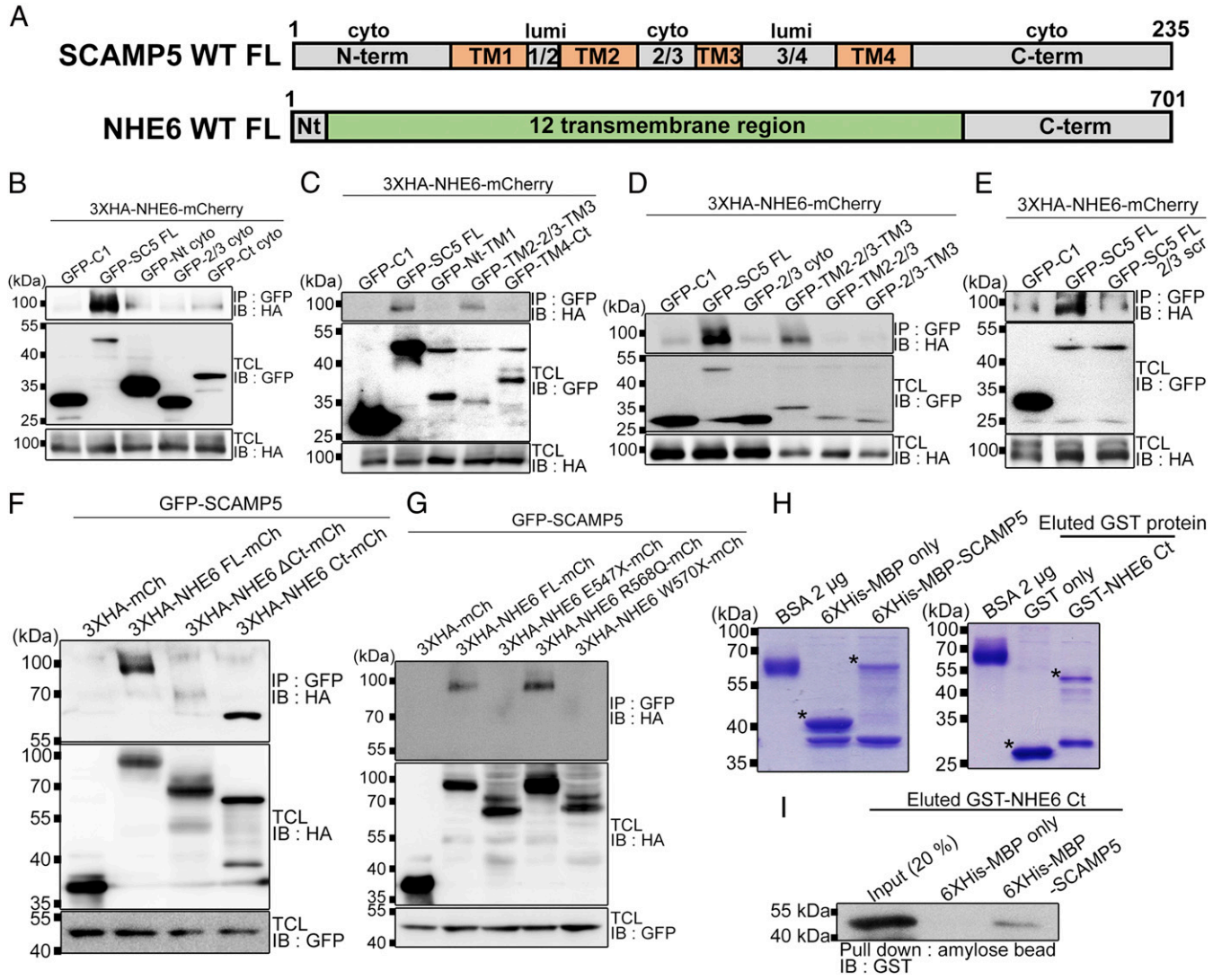

Fig. 1. NHE6 and SCAMP5 directly associate with each other. (*A*) Schematic illustration of NHE6 and SCAMP5 wild-type full-length (WT FL) domain structure. Nt, N terminus; TM, transmembrane domain; 1/2, 1/2 loop domain; 2/3, 2/3 loop domain; 3/4, 3/4 loop domain; cyto, cytoplasmic domain; lumi, luminal domain. (*B–E*) Various 3XHA-NHE6-mCherry and GFP-tagged SCAMP5 fragments were expressed in HEK293T cells, immunoprecipitated using anti-GFP antibody, and detected using an anti-HA antibody. (*F* and *G*) GFP-SCAMP5 and 3XHA-mCherry-tagged NHE6 without the C-terminal region or only the C-terminal region or NHE6 patient-found mutants was expressed in HEK293T cells, immunoprecipitated using anti-GFP antibody, and detected using an anti-HA antibody. TCL, total cell lysates; IP, immunoprecipitation; IB, immunoblotting. (*H*) Purified proteins of only 6XHis-MBP and 6XHis-MBP-SCAMP5 (*Left*) and only GST and GST-NHE6 Ct (*Right*) were confirmed by Coomassie staining. The corresponding band of each purified protein is marked with an asterisk. BSA, bovine serum albumin. (*I*) Eluted GST-NHE6 Ct proteins were pulled down with only 6XHis-MBP or 6XHis-MBP-SCAMP5 proteins using amylose bead and detected using an anti-GST antibody.

axon in SCAMP5 KD neurons. Since SCAMP5 plays a role in SV endocytosis, we first hypothesized that NHE6 would be stranded at the plasma membrane instead of being retrieved during endocytosis in SCAMP5 KD neurons. We transfected neurons with 3XHA-NHE6-mCherry in which HA tag is exposed extracellularly and stained with anti-HA antibody without permeabilization. We found that NHE6 was not detected at the cell surface in SCAMP5 KD as well as in control neurons (*SI Appendix*, Fig. S6 *A* and *B*), so this ruled out the first possibility.

Aberrant localization would be the consequence of impaired axonal trafficking of NHE6 in SCAMP5 KD neurons. After being synthesized in the cell body, NHE6 is transported along the axon to its destination, and SCAMP5 may play a role in this step. To observe the NHE6 trafficking along the axons, we cotransfected neurons with 3XHA-NHE6-mCherry, synaptophysin, and shRNA SCAMP5 or scrambled RNA and analyzed the mobility properties of NHE6 in SCAMP5 KD and control neurons by using live-cell imaging (Fig. 3*A*). We found a significant increase in the number of stationary NHE6 at the expense of the number of mobile NHE6 in SCAMP5 KD neurons while the anterograde-to-retrograde ratio was not altered (Fig. 3 *B–D*). Also, SCAMP5 KD significantly reduced the percent time in motion, segmental run length, and segmental velocity of NHE6 compared to control neurons (Fig. 3 *E–G*). Together, these results indicate that SCAMP5 KD induced the defects in axonal trafficking of NHE6.

The Synaptic Vesicle Lumen Is Hyperacidified in SCAMP5 KD Neurons. Since NHE6 dissipates ΔpH and increases Δψ across the SV membrane, we hypothesized that the perturbed localization of NHE6 in SCAMP5 KD neurons would lead to hyperacidification of the SV lumen. To measure the luminal pH of SVs, we utilized the Förster resonance energy transfer (FRET)-based ratiometric

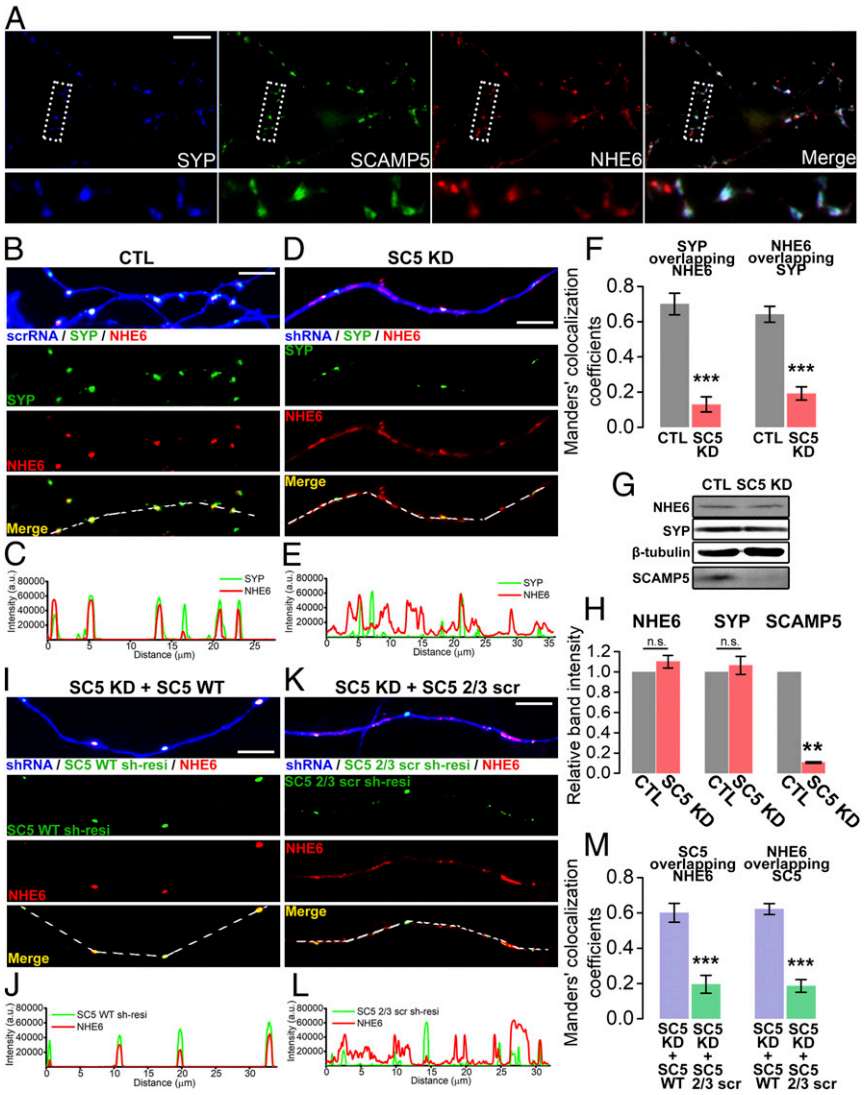

Fig. 2. SCAMP5 deficiency interferes with localization of NHE6 to SVs, which is rescued by shRNA-resistant wild-type SCAMP5. (*A*) Representative images of cultured rat hippocampal neurons cotransfected with GFP-SYP (SYP), BFP-SCAMP5 (SCAMP5), and mCherry-NHE6 (NHE6). (Scale bar, 10 μm.) (*B*, *D*, *I*, *K*) Representative images of cultured rat hippocampal neurons cotransfected with BFP-scrRNA or shRNA SCAMP5, GFP-SYP (SYP) or the shRNA-resistant form of SCAMP5, and mCherry-NHE6. The dashed line is used for line scan analysis. (Scale bar, 5 μm.) (*C*, *E*, *J*, *L*) Fluorescent intensity profiles of the respective protein along the dashed line. a.u., arbitrary units. (*F*) Manders's colocalization coefficients calculated from control (CTL) and SC5 KD neurons. SYP overlapping NHE6, CTL, 0.700 ± 0.061, $n = 5$ (coverslips). SC5 KD, 0.130 ± 0.043, $n = 8$ (coverslips), $P = 6.35E\text{-}05$; NHE6 overlapping SYP, CTL, 0.642 ± 0.045, $n = 5$ (coverslips). SC5 KD, 0.192 ± 0.038, $n = 8$ (coverslips), $P = 5.84E\text{-}05$, analyzed by Student's *t* test. (*G*) Cultured hippocampal neurons were treated with adeno-associated virus (AAV) containing SCAMP5 shRNA (SC5 KD) or scrambled RNA (CTL) and lysed for immunoblotting with the respective antibody. (*H*) Normalized relative band intensity. NHE6, CTL, 1 ± 0 (normalized), $n = 3$ (independent experiments); SC5 KD, 1.101 ± 0.062, $n = 3$ (independent experiments), $P = 0.180$; SYP, CTL, 1 ± 0 (normalized), $n = 3$ (independent experiments); SC5 KD, 1.066 ± 0.089, $n = 3$ (independent experiments), $P = 0.502$; SCAMP5, CTL, 1 ± 0 (normalized), $n = 3$ (independent experiments); SC5 KD, 0.106 ± 0.008, $n = 3$ (independent experiments), $P = 0.003$, analyzed by Student's *t* test. (*M*) Manders's colocalization coefficients calculated from SC5 KD + SC5 WT and SC5 KD + SC5 2/3 scr neurons. SC5 overlapping NHE6, SC5 KD + SC5 WT, 0.601 ± 0.054, $n = 7$ (coverslips). SC5 KD + SC5 2/3 scr, 0.196 ± 0.051, $n = 6$ (coverslips), $P = 0.0002$; NHE6 overlapping SC5, SC5 KD + SC5 WT, 0.622 ± 0.031, $n = 7$ (coverslips). SC5 KD + SC5 2/3 scr, 0.186 ± 0.036, $n = 6$ (coverslips), $P = 1.65E\text{-}06$, analyzed by Student's *t* test. Values are indicated as mean ± SEM; $^{**}P < 0.01$, $^{***}P < 0.001$.

pH-sensitive biosensor, pH-Lemon (Fig. 4*A*), that is optimized for live-cell imaging of pH conditions within acidic compartments (33). First, we transfected COS-7 cells with pH-Lemon-GPI, which targets the secretory vesicles from the Golgi and the plasma membrane (33), and measured pH-dependent ratiometric fluorescent changes of pH-Lemon at the cell surface by perfusing a nonpermeable solution of different pH (Fig. 4 *B* and *C*). We found that the half-maximal effective concentration (EC_{50}) of the mTurquoise2/FRET ratio of pH-Lemon was 6.11 (Fig. 4*D*). To express pH-Lemon in SVs, we tagged pH-Lemon to the N terminus of synaptotagmin 1 with a tobacco etch virus (TEV) protease cleavage site between them (pH-Lemon-TEV-Syt1) (Fig. 4*E*). We confirmed that pH-Lemon-TEV-Sty1 was expressed in SVs of cultured hippocampal neurons (*SI Appendix*, Fig. S7 *A* and *B*). We then removed the surface fraction of pH-Lemon-TEV-Syt1 by applying a nonpermeable TEV protease solution (*SI Appendix*, Fig. S7 *C–H*), which allowed us to observe the pH-Lemon signals emanated only from SVs. Using this probe, we found that the luminal pH of SVs in SCAMP5 KD neurons was significantly lower than that in control neurons (Fig. 4 *F–I* and *N*).

To validate whether this change is mediated by NHE6 mislocalization in SCAMP5 KD neurons, we decided to compare

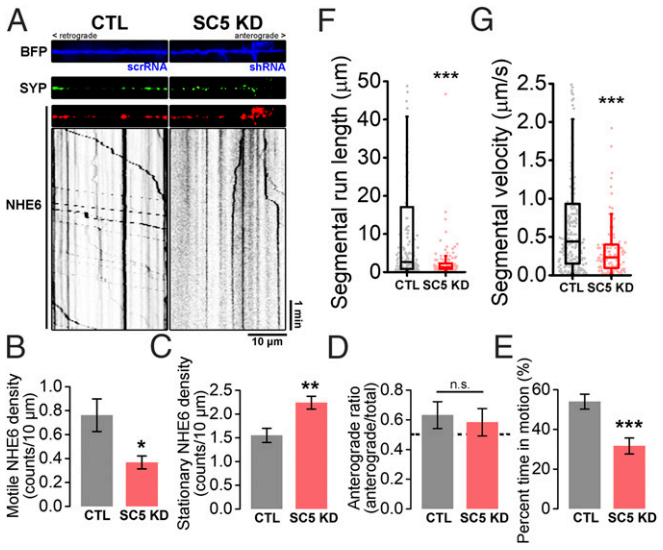

Fig. 3. SCAMP5 is important for regulating axonal trafficking of NHE6. (*A*) Representative images of cultured rat hippocampal neurons cotransfected with BFP-scrRNA or shRNA SCAMP5, GFP-SYP, and mCherry-NHE6. The kymograph for NHE6 axonal trafficking was generated from time-lapse images which were acquired at 0.5 Hz (1 frame/2 s). (*B*) Motile NHE6 density (motile NHE6 counts per 10 μm axon), CTL, 0.762 ± 0.136 counts/10 μm, $n = 17$ (axons, 9 coverslips); SC5 KD, 0.367 ± 0.054 counts/10 μm, $n = 16$ (axons, 9 coverslips), $P = 0.013$, analyzed by Student's t test. (*C*) Stationary NHE6 density (stationary NHE6 counts per 10 μm axon), CTL, 1.550 ± 0.149 counts/10 μm, $n = 17$ (axons, 9 coverslips); SC5 KD, 2.240 ± 0.135 counts/10 μm, $n = 16$ (axons, 9 coverslips), $P = 0.002$, analyzed by Student's t test. (*D*) Anterograde ratio of NHE6 trafficking (anterograde/anterograde and retrograde), CTL, 0.631 ± 0.091, $n = 17$ (axons, 9 coverslips); SC5 KD, 0.583 ± 0.092, $n = 16$ (axons, 9 coverslips), $P = 0.712$, analyzed by Student's t test. The value of the dashed line is 0.5. (*E*) Percentage of time in motion of individual motile NHE6, CTL, 54.038 ± 3.751%, $n = 88$ (counts of motile NHE6, 17 axons, 9 coverslips); SC5 KD, 31.656 ± 4.033%, $n = 46$ (counts of motile NHE6, 16 axons, 9 coverslips), $P = 2.556E\text{-}4$, analyzed by Student's t test. Values are indicated as mean ± SEM. (*F*) Box and whiskers with scattered dot graph representing segmental run length (μm) of motile NHE6. Box values are median and quartiles (25 to 75), with each scattered dot indicating individual segmental run length of motile NHE6. CTL, 2.666 ± 2.399 μm, $n = 183$ (segments, 9 coverslips); SC5 KD, 1.266 ± 0.733 μm, $n = 112$ (segments, 9 coverslips), Median ± MAD (median absolute deviation), $P = 0.6E\text{-}05$, analyzed by Mann–Whitney U test. (*G*) Box and whiskers with scattered dot graph representing segmental velocity (μm/s) of motile NHE6. Box values are median and quartiles (25 to 75), with each scattered dot indicating individual segmental velocity of motile NHE6. CTL, 0.441 ± 0.359 μm/s, $n = 183$ (segments, 9 coverslips); SC5 KD, 0.233 ± 0.143 μm/s, $n = 112$ (segments, 9 coverslips), median ± MAD, $P = 0.6E\text{-}05$, analyzed by Mann–Whitney U test. $^*P < 0.05$, $^{**}P < 0.01$, $^{***}P < 0.001$. n.s., not significant.

the SV pH between SCAMP5 KD in the background of NHE6 KO and solely SCAMP5 KD or NHE6 KO neurons. NHE6 protein was knocked out by using CRISPR-Cas9. We designed guide RNA (gRNA) against the fourth exon of NHE6 (gene: *SLC9A6*; see *Materials and Methods* for details), and GFP-pX458 (GFP-SpCas9-NLS) (34) or the NHE6 KO vector (GFP-NHE6 gRNA) with a plasmid encoding GFP was delivered into the embryonic day 17 (E17) rat hippocampus by in utero electroporation (35) (*SI Appendix*, Fig. S8*B*). Genomic DNA cleavage and NHE6 protein KO by the CRISPR-Cas9 system were validated through surveyor assay (36), immunoblotting by using the isolated hippocampal CA1 region (*SI Appendix*, Fig. S8 *C–E*), and immunocytochemistry (ICC) (*SI Appendix*, Fig. S8 *F* and *G*).

We then cotransfected pH-Lemon-TEV-Syt1 along with shRNA SCAMP5 or scrambled RNA into NHE6 KO neurons at days in vitro (DIV) 8 to 10, and the luminal pH of SVs was measured at DIV 14 to 16 (*SI Appendix*, Figs. S8*H* and S9). The efficiency of SCAMP5 KD in NHE6 KO cells was confirmed by immunoblotting and ICC in mouse hippocampal cell line HT-22 and cultured rat hippocampal neurons, respectively (*SI Appendix*, Fig. S10 *A–C*). We found that the luminal pHs of SVs in NHE6 KO and SCAMP5 KD + NHE6 KO neurons were significantly lower than that in control neurons (Fig. 4 *J–N*). However, SCAMP5 KD + NHE6 KO did not reduce the SV pH any further than NHE6 KO or SCAMP5 KD. These results indicate that the loss of NHE6 occluded the effect of SCAMP5 KD. Together, our results show that the luminal pH of SVs is regulated through proper NHE6 localization mediated by SCAMP5, and ectopic mislocalization of NHE6 in SCAMP5 KD neurons is responsible for hyperacidification of the SV lumen.

SCAMP5 Deficiency Leads to Decreased Glutamate Release at the Presynaptic Bouton. Since the conversion of ΔpH into Δψ is associated with glutamate uptake into SVs, the hyperacidification of SV lumen in SCAMP5 KD neurons might be accompanied by a lowering of Δψ and a consequent reduction in glutamate loading into SVs at glutamatergic synapses. To address this possibility, we measured the amount of glutamate released at individual presynaptic boutons by using an intensity-based fluorescent glutamate sensor, iGluSnFR (37), and analyzed the iGluSnFR responses to spontaneous glutamate release (*SI Appendix*, Fig. S11*A*) and a single action potential (AP) (*SI Appendix*, Fig. S11*D*). We found that the amplitude histogram of spontaneous iGluSnFR responses was fitted with a single Gaussian distribution (*SI Appendix*, Fig. S13*A*), implying that the unit response was reliably detected. We then cotransfected iGluSnFR along with shRNA SCAMP5 or scrambled RNA into cultured hippocampal neurons (Fig. 5 *A* and *D*) and found that the amounts of glutamate released spontaneously and evoked by a single AP were significantly lower in SCAMP5 KD neurons (Fig. 5 *C* and *F*). The reduced glutamate release in SCAMP5 KD neurons was fully rescued by introducing shRNA-resistant wild-type SCAMP5 but not by shRNA-resistant SCAMP5 with the scrambled 2/3 loop (Fig. 5 *C* and *F* and *SI Appendix*, Fig. S11 *B*, *C*, *E*, and *F*). We further showed that iGluSnFR responses to spontaneous glutamate release were also reduced in NHE6 KO, and SCAMP5 KD + NHE6 KO did not reduce iGluSnFR responses any more than NHE6 KO or SCAMP5 KD (Fig. 5 *G–I*), again indicating that the loss of NHE6 occluded the effect of SCAMP5 KD. The amplitude distribution of iGluSnFR responses in SCAMP5 KD, NHE6 KO, and SCAMP5 KD + NHE6 KO neurons was also fitted with a single Gaussian distribution but was shifted to the left compared to that in control neurons, confirming the reduction of quantal size (*SI Appendix*, Fig. S13 *A–E*).

There is a possibility that the surface localization of iGluSnFR can be affected in SCAMP5 KD neurons. To rule out this possibility, neurons transfected with iGluSnFR were treated with 100 μM glutamate (F_{100}) to increase surface iGluSnFR fluorescence maximally and pH 4 nonpermeable solution (F_{pH4}) to completely quench the surface fraction of iGluSnFR at resting state. We then measured iGluSnFR responses with a subsaturating concentration of glutamate (5 μM, F_5) (*SI Appendix*, Fig. S12 *A–D*). We found that the iGluSnFR fluorescence levels at resting state (F_0), the responsiveness of surface iGluSnFR to a saturating concentration of glutamate (ΔF_{100}), and the ratios of the surface to the internal fraction of iGluSnFR were similar in control and SCAMP5 KD neurons (*SI Appendix*, Fig. S12 *E* and *F*). In addition, the iGluSnFR responses to 5 μM glutamate normalized to the baseline fluorescence ($\Delta F_5/F_0$) were similar and constant regardless of variation in the surface iGluSnFR levels in both neurons (*SI Appendix*, Fig. S12 *G* and *H*). Together, these indicate that the surface localization of iGluSnFR was not affected by SCAMP5 KD, and the reduced iGluSnFR response in SCAMP5 KD neurons was not due to the reduced surface expression of iGluSnFR or any defects in the responsiveness of iGluSnFR.

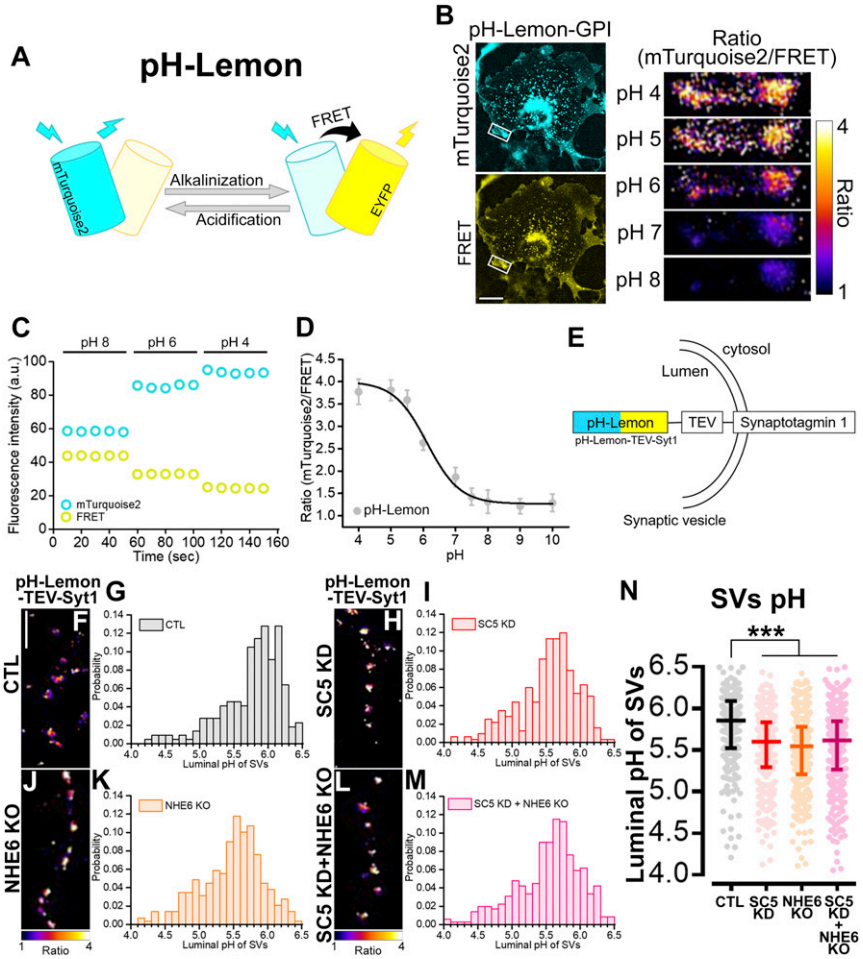

Fig. 4. Hyperacidification of SV luminal pH in SCAMP5 KD, NHE6 KO, and SCAMP5 KD + NHE6 KO neurons. (*A*) Schematic illustration of the FRET-based ratiometric pH-sensitive biosensor, pH-Lemon, consisting of mTurquoise2 and EYFP. (*B*) Representative separate images from mTurquoise2 and the FRET channel of pH-Lemon-GPI in COS-7 cells. Part of the white box in the COS-7 cell on the *Left* is magnified on the *Right*, representing the fluorescence ratio (mTurquoise2/FRET) at various pH values from pH 4 to pH 8. (Scale bar, 10 μm.) (*C*) Fluorescent intensity of donor (mTurquoise2) and FRET images of pH-Lemon-GPI in COS-7 cells perfused with various pH ranges of nonpermeable extracellular solution. (*D*) Dose–response relationship curve of pH-Lemon (n = 7, mean ± SD). (*E*) Schematic illustration of DNA plasmid construction of pH-Lemon-TEV-Syt1. (*F*, *H*, *J*, *L*) Representative images of the mTurquoise2/FRET ratio of pH-Lemon-TEV-Syt1 in control, SCAMP5 KD, NHE6 KO, and SCAMP5 KD + NHE6 KO neurons, respectively. (Scale bar, 5 μm.) (*G*, *I*, *K*, *M*) Histogram graphs of the luminal pH of SVs obtained from the mTurquoise2/FRET ratio value in CTL, n = 219 (boutons); SC5 KD, n = 318 (boutons); NHE6 KO, n = 289 (boutons); and SC5 KD + NHE6 KO, n = 356 (boutons). (*N*) Scattered dot graph representing the luminal pH of SVs. Values are median and quartiles (25 to 75) of SVs pH, with each scattered dot indicating individual pH at one bouton. CTL, 5.854 ± 0.261 pH units, n = 219 (boutons, 10 coverslips); SC5 KD, 5.599 ± 0.259 pH units, n = 318 (boutons, 15 coverslips); NHE6 KO, 5.546 ± 0.270 pH units, n = 289 (boutons, 13 coverslips); SC5 KD + NHE6 KO, 5.615 ± 0.268 pH units, n = 356 (boutons, 17 coverslips), P = 7.461E-15, analyzed by a Kruskal–Wallis test followed by a Mann–Whitney U post hoc test. Values are indicated as median ± MAD, ***P < 0.001.

We further verified the quantal size change by using electrophysiological recordings of cultured autaptic neurons infected with adeno-associated virus containing shRNA SCAMP5 or scrambled RNA. Whole-cell patch-clamp was carried out to measure mEPSC (miniature excitatory postsynaptic current), eEPSC (evoked excitatory postsynaptic current), and mIPSC (miniature inhibitory postsynaptic current) in the control, SCAMP5 KD, NHE6 KO, and SCAMP5 KD + NHE6 KO neurons (Fig. 6 *A* and *D* and *SI Appendix*, Fig. S14*A*). The amplitudes of both mEPSC and eEPSC were significantly decreased in SCAMP5 KD, NHE6 KO, and SCAMP5 KD + NHE6 KO neurons (Fig. 6 *B* and *E*), while the amplitude of mIPSC was not altered (*SI Appendix*, Fig. S14*B*). The frequency of mEPSC or mIPSC appeared to be lower in SCAMP5 KD, NHE6 KO, and SCAMP5 KD + NHE6 KO neurons compared to that in control neurons, but differences were not statistically significant (Fig. 6*C* and *SI Appendix*, Fig. S14*C*). All these results indicate a decrease in the quantal size of SCAMP5 KD neurons, which is due to the reduction in the luminal pH of SVs following the perturbed localization of NHE6.

Discussion

Our results reveal an interaction between SCAMP5 and NHE6 that regulates axonal trafficking and synaptic localization of NHE6. Their interaction is critical for controlling the strength of synaptic transmission by modulating the luminal pH of SVs and the quantal size of glutamate release at individual presynaptic boutons. Previous studies using rat brain synaptosomes and the calyx of Held showed that SVs contain monovalent cation/H^+ exchangers that convert ΔpH into Δψ, which promotes glutamate uptake into SVs (15, 16, 38). However, how NHEs are recruited to SVs remained unknown. In this study, we found that the interaction of the C-terminal region of NHE6 with the 2/3 loop domain of SCAMP5 (Fig. 1) is critical for the recruitment of NHE6 to SVs (Fig. 2 and *SI Appendix*, Figs. S3–S5).

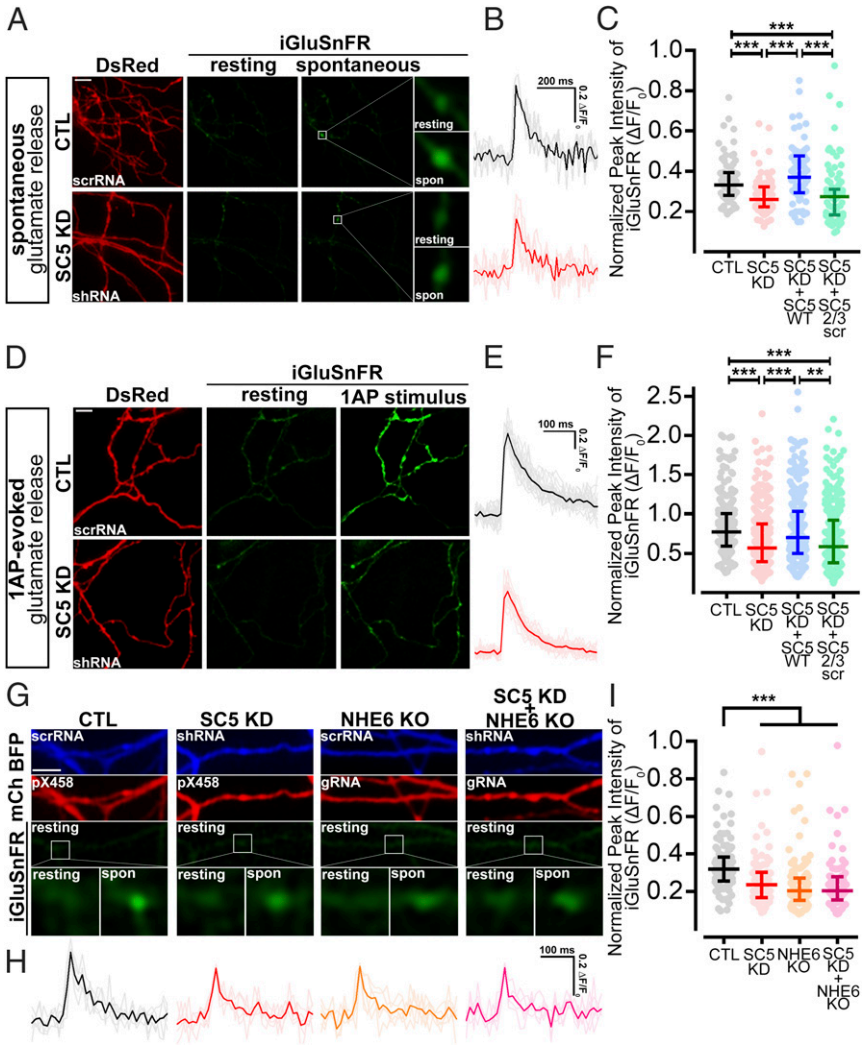

Fig. 5. The amount of spontaneous and evoked glutamate release is reduced in SC5 KD neurons. (*A* and *D*) Representative images of cultured hippocampal neurons cotransfected with DsRed-scrRNA or shRNA SCAMP5 and iGluSnFR. Images of iGluSnFR represent the resting state and the response of glutamate released spontaneously or by a single AP stimulus. (Scale bar, 5 μm.) (*B* and *E*) Representative traces of individual response (thin colored lines) and average trace (thick colored lines) of the iGluSnFR signal during spontaneous or evoked glutamate release at one presynaptic bouton in CTL and SC5 KD neurons. (*C*) Scattered dot graph representing normalized peak intensity of iGluSnFR ($\Delta F/F_0$) during spontaneous glutamate release. Values are median and quartiles (25 to 75) of iGluSnFR responses, with each scattered dot indicating the individual response at one bouton. CTL, 0.332 ± 0.057 $\Delta F/F_0$, $n = 73$ (boutons, 8 coverslips); SC5 KD, 0.260 ± 0.049 $\Delta F/F_0$, $n = 90$ (boutons, 9 coverslips); SC5 KD + SC5 WT, 0.370 ± 0.091 $\Delta F/F_0$, $n = 71$ (boutons, 9 coverslips); SC5 KD + SC5 2/3 scr, 0.274 ± 0.079 $\Delta F/F_0$, $n = 96$ (boutons, 11 coverslips), $P = 1.075E\text{-}10$, analyzed by a Kruskal–Wallis test followed by a Mann–Whitney *U* post hoc test. (*F*) Scattered dot graph representing normalized peak intensity of iGluSnFR ($\Delta F/F_0$) during evoked glutamate release. Values are median and quartiles (25 to 75) of iGluSnFR responses, with each scattered dot indicating individual response at one bouton. CTL, 0.770 ± 0.206 $\Delta F/F_0$, $n = 262$ (boutons, 17 coverslips); SC5 KD, 0.570 ± 0.219 $\Delta F/F_0$, $n = 298$ (boutons, 19 coverslips); SC5 KD + SC5 WT, 0.697 ± 0.235 $\Delta F/F_0$, $n = 315$ (boutons, 22 coverslips); SC5 KD + SC5 2/3 scr, 0.587 ± 0.238 $\Delta F/F_0$, $n = 305$ (boutons, 21 coverslips), $P = 1.894E\text{-}12$, analyzed by a Kruskal–Wallis test followed by a Mann–Whitney *U* post hoc test. Values are indicated as median ± MAD. (*G*) Representative images of cultured hippocampal NHE6 KO or control neurons cotransfected with BFP-scrRNA or shRNA SCAMP5 and iGluSnFR. Images of iGluSnFR represent the resting state and the response of glutamate released spontaneously. (Scale bar, 5 μm.) (*H*) Representative traces of individual response (thin colored lines) and average trace (thick colored lines) of the iGluSnFR signal during spontaneous glutamate release at one presynaptic bouton in CTL, SC5 KD, NHE6 KO, and SC5 KD + NHE6 KO neurons. (*I*) Scattered dot graph representing normalized peak intensity of iGluSnFR ($\Delta F/F_0$) during spontaneous glutamate release. Values are median and quartiles (25 to 75) of iGluSnFR responses, with each scattered dot indicating individual response at one bouton. CTL, 0.319 ± 0.063 $\Delta F/F_0$, $n = 111$ (boutons, 10 coverslips); SC5 KD, 0.236 ± 0.067 $\Delta F/F_0$, $n = 75$ (boutons, 7 coverslips); NHE6 KO, 0.204 ± 0.062 $\Delta F/F_0$, $n = 109$ (boutons, 10 coverslips); SC5 KD + NHE6 KO, 0.204 ± 0.057 $\Delta F/F_0$, $n = 80$ (boutons, 8 coverslips), $P = 1.891E\text{-}13$, analyzed by a Kruskal–Wallis test followed by a Mann–Whitney *U* post hoc test. Values are indicated as median ± MAD; $^{**}P < 0.01$, $^{***}P < 0.001$.

SCAMP1 and 2 are known to interact with NHE5 on the cell surface (27) and NHE7 on the Golgi apparatus (28), respectively. Intriguingly, SCAMP2 does not interact with NHE6 (28), and SCAMP5 does not interact with NHE5 (27). This interaction specificity could be due to the divergent C-terminal domains of NHE isoforms (14), indicating that the C-terminal region of NHEs determines the SCAMP isoforms that interact with it, and SCAMPs serve as the selective carriers of NHEs for their targeting to destined cellular organelles. This idea is fully consistent with our results that without SCAMP5 interaction, NHE6 failed to be localized at its destination. In addition, we found that several C-terminally truncated mutant forms of NHE6 (E547X, W570X) failed to bind to SCAMP5. This result suggests the possibility that other nonsense mutants of NHE6 without a C terminus, such as E64X and W523X (11), Q306X (39), Q407X (40), and R500X (41), cannot interact with SCAMP5 and that the failure to do so

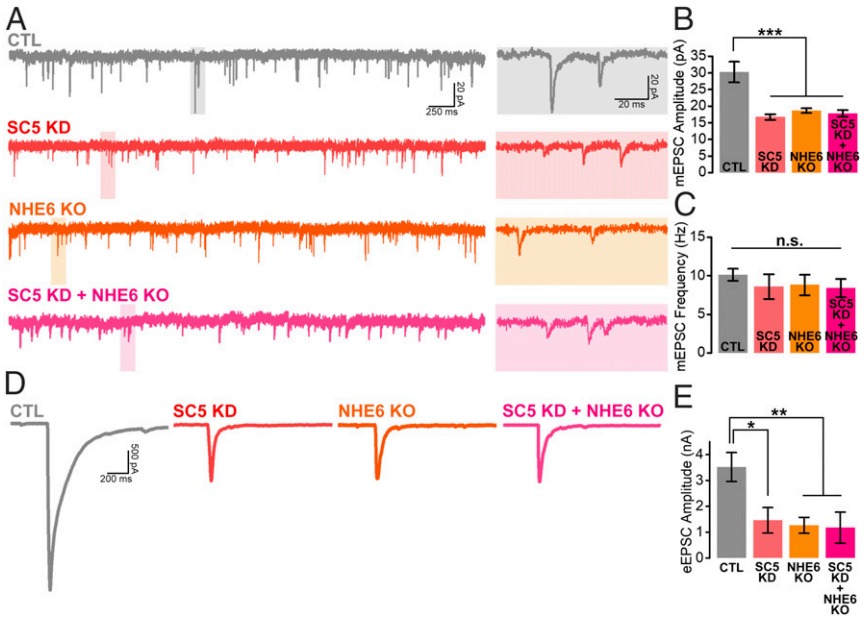

Fig. 6. Glutamatergic neurotransmission is impaired in SC5 KD, NHE6 KO, and SC5 KD + NHE6 KO neurons. (*A* and *D*) Representative traces of mEPSC and eEPSC in CTL, SC5 KD, NHE6 KO, and SC5 KD + NHE6 KO neurons, respectively. (*B*) Average amplitude of mEPSC in CTL, SC5 KD, NHE6 KO, and SC5 KD + NHE6 KO neurons. CTL, 30.257 ± 3.093 pA, $n = 6$ (coverslips); SC5 KD, 16.735 ± 0.837 pA, $n = 5$ (coverslips); NHE6 KO, 18.628 ± 0.705 pA, $n = 5$ (coverslips); SC5 KD + NHE6 KO, 17.815 ± 0.996 pA, $n = 5$ (coverslips); $F_{(3,\ 17)} = 11.685$, $P = 0.0002$, analyzed by a one-way ANOVA test followed by a least significant difference (LSD) post hoc test. (*C*) Average frequency of mEPSC in CTL, SC5 KD, NHE6 KO, and SC5 KD + NHE6 KO neurons. CTL, 10.111 ± 0.783 Hz, $n = 6$ (coverslips); SC5 KD, 8.600 ± 1.600 Hz, $n = 5$ (coverslips); NHE6 KO, 8.800 ± 1.319 Hz, $n = 5$ (coverslips); SC5 KD + NHE6 KO, 7.200 ± 1.356 Hz, $n = 5$ (coverslips); $F_{(3,\ 17)} = 0.933$, $P = 0.446$, analyzed by a one-way ANOVA test followed by a LSD post hoc test. (*E*) Average amplitude of eEPSC in CTL, SC5 KD, NHE6 KO, and SC5 KD + NHE6 KO neurons. CTL, 3.519 ± 0.561 nA, $n = 5$ (coverslips); SC5 KD, 1.459 ± 0.493 nA, $n = 5$ (coverslips); NHE6 KO, 1.265 ± 0.308 nA, $n = 5$ (coverslips); SC5 KD + NHE6 KO, 1.174 ± 0.599 nA, $n = 5$ (coverslips); $F_{(3,\ 16)} = 4.920$, $P = 0.013$, analyzed by a one-way ANOVA test followed by a LSD post hoc test. Values are indicated as mean ± SEM; $*P < 0.05$, $**P < 0.01$, $***P < 0.001$. n.s., not significant.

may be the molecular mechanism underpinning several neuropsychiatric and neurodevelopmental disorders.

iGluSnFR has been used for imaging activity from somas and dendritic spines in vivo (37, 42) and axonal boutons in slices (43). The signal-to-noise ratio (SNR) of iGluSnFR is high enough to reliably quantify the amount of glutamate released from SVs by spontaneous SV fusion or in response to a single AP. Although previous studies have visualized individual presynaptic fusion events using pHluorin-based probes and FM dyes, the suboptimal SNR of these probes requires estimates made from the pooled average of multiple responses or a train of stimuli to assess presynaptic properties (44–46). In addition, iGluSnFR responses reflect the actual amount of glutamate released while other presynaptic probes only reveal the vesicular trafficking processes. Our data suggest that iGluSnFR is an excellent presynaptic activity indicator, especially for the measurement of glutamate release in response to APs. The iGluSnFR or other sensitive presynaptic probes would help to provide more information about presynaptic changes during synaptic plasticity.

Previous work has shown that the receptor for activated C kinase 1 (RACK1) plays a role in regulating the distribution of NHE6 between endosomes and the plasma membrane (29, 47). RACK1 serves as a shuttling protein, enabling the various kinases, including PKCβII, Fyn, and Src, to phosphorylate their substrate at the appropriate locations (48). NHE6 interacts with RACK1 via its C-terminal cytoplasmic region (29), and the same region mediates the interaction with SCAMP5. These results suggest that NHE6 can use different carriers to be localized to other organelles. It is of interest to see whether SCAMP5 and RACK1 compete with each other for binding to NHE6, and if so, the phosphorylation or posttranslational modification pattern of NHE6 could alter its binding preference.

NHE6 and SCAMP5 are both SV transmembrane proteins and could be present on the SVs of other types of neurons. According to previous studies, SCAMP5 is involved in the endocytic pathway in mouse striatal neurons (49), and NHE6 has been detected by mass spectrometry on the SVs of GABAergic neurons (18). Although we found that the amplitude and frequency of mIPSC were not altered in cultured SCAMP5 KD and NHE6 KO hippocampal neurons, it would be of interest to study whether the interaction between NHE6 and SCAMP5 also regulates the quantal size of GABA release at GABAergic synapses in vivo.

In this study, we identified the functional linkage between SCAMP5 and NHE6, both of which are autism candidate genes (9, 22). Thus, our results raised the intriguing possibility that defects in the interaction between SCAMP5 and NHE6 could underlie some of the pathological features of autism spectrum disorder (ASD). In addition, loss-of-function mutations of NHE6 are involved in the formation of deposits of tau (50), localization of amyloid precursor protein, and the process from production to clearance of beta-amyloid protein (51), all of which are implicated in Alzheimer's disease (AD). Our findings suggest the intriguing possibility that defects in NHE6 recruitment into SVs due to impaired interaction between NHE6 and SCAMP5 are responsible for the synaptic dysfunction observed in autism and AD.

Materials and Methods

Plasmid DNA Construction. Plasmid DNA constructs used in this research are described in detail in *SI Appendix, Materials and Methods* and Table S1

Western Blot and Immunoprecipitation. HEK293T and HT-22 cells were transfected with different constructs according to experiments using Lipofectamine 2000

(Invitrogen). Two days after transfection, Western blot and immunoprecipitation were performed as described in detail in *SI Appendix, Materials and Methods*.

Neuron Transfection, Image Acquisition, and Immunocytochemistry. Hippocampal neurons were transfected by using the calcium-phosphate method and imaged at DIV 14 to 16. For immunocytochemistry, neurons were fixed in 4% paraformaldehyde with 4% sucrose/phosphate-buffered saline (PBS) or 3% glyoxal with 20% absolute ethanol and 7.5% acetic acid. Detailed processes are described in *SI Appendix, Materials and Methods*.

In Utero Electroporation. CRISPR-Cas9 plasmids were delivered to E17 fetal Sprague–Dawley rats by in utero electroporation, and the detailed processes are described in *SI Appendix, Materials and Methods*.

Calibration and Calculation of Luminal pH of Synaptic Vesicle. The luminal pH of SVs was measured by using the pH-Lemon DNA construct as previously described (33), and the detailed processes are described in *SI Appendix, Materials and Methods*.

Autaptic Neuron Culture and Electrophysiology. Rat hippocampal autaptic neurons were prepared, and electrophysiological recordings were performed as previously described (26, 52). The detailed processes are described in *SI Appendix, Materials and Methods*.

Image Acquisition of Glutamate Release Using iGluSnFR. Transfected neurons with iGluSnFR at DIV 14 to 16 were mounted in a perfusion/stimulation chamber (Chamlide) on the stage of a Nikon Eclipse Ti-U fluorescence microscope, and the detailed processes are described in *SI Appendix, Materials and Methods*.

Statistical Analysis. For analysis of protein colocalization, Manders's colocalization coefficients were calculated using ImageJ (NIH) with the JACoP plug-in function (https://imagej.nih.gov/ij/plugins/track/jacop.html). Quantitative measurements of iGluSnFR responses from individual boutons were obtained using ImageJ (NIH). Electrophysiological recording data were analyzed and plotted using IGOR Pro (Wavemetrics), MiniAnalysis software (Synaptosoft), and Origin 9 software (OriginLab). Significances of all data are reported as $*P < 0.05$, $**P < 0.01$, $***P < 0.001$, and the detailed processes are described in *SI Appendix, Materials and Methods*.

Data Availability. All experimental protocols are described in the *Materials and Methods* section or in the references therein. Sources of all plasmids, cell lines, and antibodies used in this study, and all study data are included in the article and in *SI Appendix*.

ACKNOWLEDGMENTS. We thank Dr. Rajini Rao (Johns Hopkins University, Baltimore, MD) for providing the human NHE6 cDNA construct. We also thank Soohyun Kim for help with the analysis of the iGluSnFR experiment, Ji Yun Jang for help with time-lapse imaging of NHE6 trafficking and immunocytochemistry, and Hyoung Ro Lee for help with the in utero electroporation experiment. This work was supported by grants from the National Research Foundation of Korea (Grants 2019R1A2C2089182 and 2017M3C7A1044958 to S.C.). This work was also supported by Grant 800-20180489 and the Education and Research Encouragement Fund of Seoul National University Hospital.

1. S. Takamori, Presynaptic molecular determinants of quantal size. *Front. Synaptic Neurosci.* **8**, 2 (2016).
2. S. Saroussi, N. Nelson, Vacuolar H(+)-ATPase-an enzyme for all seasons. *Pflugers Arch.* **457**, 581–587 (2009).
3. R. H. Edwards, The neurotransmitter cycle and quantal size. *Neuron* **55**, 835–858 (2007).
4. R. D. Blakely, R. H. Edwards, Vesicular and plasma membrane transporters for neurotransmitters. *Cold Spring Harb. Perspect. Biol.* **4**, a005595 (2012).
5. J. Orlowski, S. Grinstein, Diversity of the mammalian sodium/proton exchanger SLC9 gene family. *Pflugers Arch.* **447**, 549–565 (2004).
6. C. L. Brett, M. Donowitz, R. Rao, Evolutionary origins of eukaryotic sodium/proton exchangers. *Am. J. Physiol. Cell Physiol.* **288**, C223–C239 (2005).
7. J. R. Casey, S. Grinstein, J. Orlowski, Sensors and regulators of intracellular pH. *Nat. Rev. Mol. Cell Biol.* **11**, 50–61 (2010).
8. P. Strømme *et al.*, X-linked Angelman-like syndrome caused by Slc9a6 knockout in mice exhibits evidence of endosomal-lysosomal dysfunction. *Brain* **134**, 3369–3383 (2011).
9. M. Schwede, K. Garbett, K. Mirnics, D. H. Geschwind, E. M. Morrow, Genes for endosomal NHE6 and NHE9 are misregulated in autism brains. *Mol. Psychiatry* **19**, 277–279 (2014).
10. J. H. Schuurs-Hoeijmakers *et al.*, Identification of pathogenic gene variants in small families with intellectually disabled siblings by exome sequencing. *J. Med. Genet.* **50**, 802–811 (2013).
11. M. F. Pescosolido *et al.*, Genetic and phenotypic diversity of NHE6 mutations in Christianson syndrome. *Ann. Neurol.* **76**, 581–593 (2014).
12. E. M. Morrow *et al.*, Identifying autism loci and genes by tracing recent shared ancestry. *Science* **321**, 218–223 (2008).
13. K. Brookes *et al.*, The analysis of 51 genes in DSM-IV combined type attention deficit hyperactivity disorder: Association signals in DRD4, DAT1 and 16 other genes. *Mol. Psychiatry* **11**, 934–953 (2006).
14. K. C. Kondapalli, H. Prasad, R. Rao, An inside job: How endosomal Na(+)/H(+) exchangers link to autism and neurological disease. *Front. Cell. Neurosci.* **8**, 172 (2014).
15. G. Y. Goh *et al.*, Presynaptic regulation of quantal size: K+/H+ exchange stimulates vesicular glutamate transport. *Nat. Neurosci.* **14**, 1285–1292 (2011).
16. H. Huang, L. O. Trussell, Presynaptic HCN channels regulate vesicular glutamate transport. *Neuron* **84**, 340–346 (2014).
17. J. C. Ullman *et al.*, A mouse model of autism implicates endosome pH in the regulation of presynaptic calcium entry. *Nat. Commun.* **9**, 330 (2018).
18. M. Grønborg *et al.*, Quantitative comparison of glutamatergic and GABAergic synaptic vesicles unveils selectivity for few proteins including MAL2, a novel synaptic vesicle protein. *J. Neurosci.* **30**, 2–12 (2010).
19. Q. Ouyang *et al.*, Christianson syndrome protein NHE6 modulates TrkB endosomal signaling required for neuronal circuit development. *Neuron* **80**, 97–112 (2013).
20. R. Fernández-Chacón, T. C. Südhof, Novel SCAMPs lacking NPF repeats: Ubiquitous and synaptic vesicle-specific forms implicate SCAMPs in multiple membrane-trafficking functions. *J. Neurosci.* **20**, 7941–7950 (2000).
21. R. Fernández-Chacón, G. Alvarez de Toledo, R. E. Hammer, T. C. Südhof, Analysis of SCAMP1 function in secretory vesicle exocytosis by means of gene targeting in mice. *J. Biol. Chem.* **274**, 32551–32554 (1999).
22. D. Castermans *et al.*, SCAMP5, NBEA and AMISYN: Three candidate genes for autism involved in secretion of large dense-core vesicles. *Hum. Mol. Genet.* **19**, 1368–1378 (2010).
23. D. Zhang *et al.*, Deficiency of SCAMP5 leads to pediatric epilepsy and dysregulation of neurotransmitter release in the brain. *Hum. Genet.* **139**, 545–555 (2020).
24. L. Hubert *et al.*, De novo SCAMP5 mutation causes a neurodevelopmental disorder with autistic features and seizures. *J. Med. Genet.* **57**, 138–144 (2020).
25. H. Zhao *et al.*, SCAMP5 plays a critical role in synaptic vesicle endocytosis during high neuronal activity. *J. Neurosci.* **34**, 10085–10095 (2014).
26. D. Park *et al.*, Impairment of release site clearance within the active zone by reduced SCAMP5 expression causes short-term depression of synaptic release. *Cell Rep.* **22**, 3339–3350 (2018).
27. G. H. Diering, J. Church, M. Numata, Secretory carrier membrane protein 2 regulates cell-surface targeting of brain-enriched Na+/H+ exchanger NHE5. *J. Biol. Chem.* **284**, 13892–13903 (2009).
28. P. J. Lin *et al.*, Secretory carrier membrane proteins interact and regulate trafficking of the organellar (Na+,K+)/H+ exchanger NHE7. *J. Cell Sci.* **118**, 1885–1897 (2005).
29. R. Ohgaki, N. Fukura, M. Matsushita, K. Mitsui, H. Kanazawa, Cell surface levels of organellar Na+/H+ exchanger isoform 6 are regulated by interaction with RACK1. *J. Biol. Chem.* **283**, 4417–4429 (2008).
30. L. Pulakat *et al.*, Ligand-dependent complex formation between the Angiotensin II receptor subtype AT2 and Na+/H+ exchanger NHE6 in mammalian cells. *Peptides* **26**, 863–873 (2005).
31. A. Piton *et al.*, Systematic resequencing of X-chromosome synaptic genes in autism spectrum disorder and schizophrenia. *Mol. Psychiatry* **16**, 867–880 (2011).
32. H. Prasad, R. Rao, The Na+/H+ exchanger NHE6 modulates endosomal pH to control processing of amyloid precursor protein in a cell culture model of Alzheimer disease. *J. Biol. Chem.* **290**, 5311–5327 (2015).
33. S. Burgstaller *et al.*, pH-lemon, a fluorescent protein-based pH reporter for acidic compartments. *ACS Sens.* **4**, 883–891 (2019).
34. F. A. Ran *et al.*, Genome engineering using the CRISPR-Cas9 system. *Nat. Protoc.* **8**, 2281–2308 (2013).
35. S. M. Kolk, A. J. de Mooij-Malsen, G. J. Martens, Spatiotemporal molecular approach of in utero electroporation to functionally decipher endophenotypes in neurodevelopmental disorders. *Front. Mol. Neurosci.* **4**, 37 (2011).
36. T. Tsuji, Y. Niida, Development of a simple and highly sensitive mutation screening system by enzyme mismatch cleavage with optimized conditions for standard laboratories. *Electrophoresis* **29**, 1473–1483 (2008).
37. J. S. Marvin *et al.*, An optimized fluorescent probe for visualizing glutamate neurotransmission. *Nat. Methods* **10**, 162–170 (2013).
38. D. Li, Y. Zhu, H. Huang, Spike activity regulates vesicle filling at a glutamatergic synapse. *J. Neurosci.* **40**, 4972–4980 (2020).
39. C. Mignot *et al.*, Novel mutation in SLC9A6 gene in a patient with Christianson syndrome and retinitis pigmentosum. *Brain Dev.* **35**, 172–176 (2013).
40. R. J. Schroer *et al.*, Natural history of Christianson syndrome. *Am. J. Med. Genet. A.* **152A**, 2775–2783 (2010).
41. G. D. Gilfillan *et al.*, SLC9A6 mutations cause X-linked mental retardation, microcephaly, epilepsy, and ataxia, a phenotype mimicking Angelman syndrome. *Am. J. Hum. Genet.* **82**, 1003–1010 (2008).

42. Y. Xie *et al*., Resolution of high-frequency mesoscale intracortical maps using the genetically encoded glutamate sensor iGluSnFR. *J. Neurosci.* **36**, 1261–1272 (2016).
43. T. P. Jensen, K. Zheng, O. Tyurikova, J. P. Reynolds, D. A. Rusakov, Monitoring single-synapse glutamate release and presynaptic calcium concentration in organised brain tissue. *Cell Calcium* **64**, 102–108 (2017).
44. J. Balaji, T. A. Ryan, Single-vesicle imaging reveals that synaptic vesicle exocytosis and endocytosis are coupled by a single stochastic mode. *Proc. Natl. Acad. Sci. U.S.A.* **104**, 20576–20581 (2007).
45. Y. Zhu, J. Xu, S. F. Heinemann, Two pathways of synaptic vesicle retrieval revealed by single-vesicle imaging. *Neuron* **61**, 397–411 (2009).
46. N. C. Harata, S. Choi, J. L. Pyle, A. M. Aravanis, R. W. Tsien, Frequency-dependent kinetics and prevalence of kiss-and-run and reuse at hippocampal synapses studied with novel quenching methods. *Neuron* **49**, 243–256 (2006).
47. F. Lucien *et al*., Hypoxia-induced mobilization of NHE6 to the plasma membrane triggers endosome hyperacidification and chemoresistance. *Nat. Commun.* **8**, 15884 (2017).
48. D. R. Adams, D. Ron, P. A. Kiely, RACK1, A multifaceted scaffolding protein: Structure and function. *Cell Commun. Signal.* **9**, 22 (2011).
49. J. Y. Noh *et al*., SCAMP5 links endoplasmic reticulum stress to the accumulation of expanded polyglutamine protein aggregates via endocytosis inhibition. *J. Biol. Chem.* **284**, 11318–11325 (2009).
50. J. Y. Garbern *et al*., A mutation affecting the sodium/proton exchanger, SLC9A6, causes mental retardation with tau deposition. *Brain* **133**, 1391–1402 (2010).
51. H. Prasad, R. Rao, Amyloid clearance defect in ApoE4 astrocytes is reversed by epigenetic correction of endosomal pH. *Proc. Natl. Acad. Sci. U.S.A.* **115**, E6640–E6649 (2018).
52. A. Burgalossi *et al*., Analysis of neurotransmitter release mechanisms by photolysis of caged Ca^{2+} in an autaptic neuron culture system. *Nat. Protoc.* **7**, 1351–1365 (2012).